



Available online at www.sciencedirect.com



ScienceDirect

Trans. Nonferrous Met. Soc. China 32(2022) 3065–3076

Transactions of
Nonferrous Metals
Society of China

www.tnmsc.cn



Mechanical properties and microstructure evolution of solidified copper tailings with hydantoin epoxy resin

Yong HE^{1,2}, Wen-qiang JIANG^{1,2}, Ke-ping CHEN^{1,2}, Lian-rong WU³,
Ke-neng ZHANG^{1,2}, Zhi-peng YU^{1,2}, Xue-ping GAN⁴, De-shan FENG^{1,2}

1. Key Laboratory of Metallogenetic Prediction of Nonferrous Metals and Geological Environment Monitoring, Ministry of Education, Central South University, Changsha 410083, China;
2. School of Geosciences and Info-Physics, Central South University, Changsha 410083, China;
3. Yunnan Diqing Nonferrous Metals Co., Ltd., Shangri-La 674400, China;
4. State Key Laboratory of Powder Metallurgy, Central South University, Changsha 410083, China

Received 15 August 2021; accepted 20 January 2022

Abstract: Based on the strength and microstructure tests, the effects of the hydantoin epoxy resin content and curing time on the mechanical properties and microstructure of copper tailings specimens were studied. The results showed that the strength of the solidified specimens was increased to 20.84 MPa with 30 wt.% addition of hydantoin epoxy resin. When the specimens with 10% hydantoin epoxy resin were cured for 7 and 14 d, the strengths were 6.33 and 6.67 MPa respectively, which met the requirements as foundation filler and building materials. The microscopic tests showed that the agglomeration was enhanced and the porosities of the solidified specimens were reduced with increase in the hydantoin epoxy resin content, which could greatly enhance the strength of solidified specimens.

Key words: copper tailings; hydantoin epoxy resin; mechanical properties; microstructure

1 Introduction

With yearly increase in the scale of mining, the quantity of tailings produced during mining is continuously increasing. Tailings are generally exposed to the surface environment for an extended period. Owing to the effect of surface water and groundwater seepage, the metallic minerals in the tailings enter the underground water and soil, creating a potential environmental problem [1–4]. In recent years, more than 40 tailings safety accidents and 9 environmental pollution accidents have occurred in China, resulting in 354 deaths [5]. According to the report of Ministry of Ecology and Environment of China, the total tailings production was 1030 Mt in 2019. However, owing to the single

utilization method or insufficient recycling of tailings, the comprehensive utilization of tailings is 280 Mt, accounting for only 27% of the total production. Therefore, it is imperative to follow effective treatment and comprehensive utilization of tailings [6].

Solidification/stabilization (S/S) is one of the most used methods to handle tailings, which utilizes the physicochemical reaction between inorganic gel materials and tailings to obtain excellent physical properties and increase the environmental safety characteristics [7–9]. At the same time, the strength characteristics of solidified tailings are the most important mechanical parameters to evaluate the effect of the treatment, and are essential to determine their utilization in engineering. Many countries have stipulated the requirements for the

Corresponding author: Ke-ping CHEN, Tel: +86-15974263943, E-mail: 1354995204@qq.com

DOI: 10.1016/S1003-6326(22)66003-5

1003-6326/© 2022 The Nonferrous Metals Society of China. Published by Elsevier Ltd & Science Press

mechanical parameters regarding the utilization of solidified tailings (for example, as base filler or building material) [10,11].

Numerous studies have been conducted on the mechanical properties and resource utilization based on the solidification of tailings. Gold mine tailings were solidified by using calcium sulfoaluminate–belite cement by KIVENTERÄ et al [12], and it was concluded that increasing the mine tailings content up to 50 wt.% of the total binder amount yielded the strength of 7.337 MPa of the specimens after 28 d. In addition, the tailings in blast furnace slag were solidified, and it was concluded that the compressive strength of the solidified product was more than 10 MPa despite the addition of 70% tailings [13]. It was reported that tailings solidified with cement and geopolymers have good physical properties and immobilize harmful components [8,14,15]. However, cement and geopolymers had poor solidifying effects when the tailings were excessively compatibilized [16,17]. At the same time, Ordinary Portland Cement (OPC) will consume large amounts of energy and be responsible for high CO₂ emissions [12,18,19]. Therefore, the research and development of new solidifying materials are particularly critical.

Heretofore, several researchers have developed new materials for solidifying tailings with excellent solidifying effect, excellent stability, and reasonable economy [20,21]. In recent years, the gel system utilizing hydantoin epoxy resin has provided a high-strength three-dimensional polymer network structure with excellent early strength and long-term stability, which can be applied to the treatment of hazardous wastes such as tailings and slag [22,23]. Currently, the application of hydantoin epoxy resin is mainly focused on the preparation of ceramics [24–26]. The Si₃N₄ green body was prepared by ZENG et al [27], who found that with increase in the hydantoin epoxy resin content from 5 wt.% to 20 wt.%, the flexural strength of the Si₃N₄ green body was enhanced from 5.3 to 31.6 MPa. Similarly, XIE et al [28] used the hydantoin epoxy resin system to obtain alumina ceramic raw blank with a strength of up to 43.4 MPa. Previous studies rarely focused on solidifying tailings with hydantoin epoxy resin; especially, the mechanical properties and micro-mechanism of tailings solidified with hydantoin

epoxy resin have not been comprehensively investigated [29,30]. Generally, the mechanical properties and microstructure evolution of solidified materials are the main parameters to assess the suitability of a solidified body as base filler and building material [31–34]. MUHAMMAD et al [35] found that the chromite ore processing residues (COPRs) were effectively solidified in composite based geopolymer and strength of 33 MPa was obtained. Similarly, ZHAO et al [36] found that the strength of solidified bodies added with 70 wt.% lead–zinc tailings (LZTs) decreased to 21.68 MPa, the microstructure of the solidified bodies was studied, and their action and mechanism were discussed by means of modern detection measures such as SEM and XRD. Therefore, it is of immense engineering significance to study the strength and micro-mechanism of tailings solidified using hydantoin epoxy resin to promote their recycling.

This study investigated the effect of hydantoin epoxy resin on the mechanical properties and micro-mechanism of solidified copper tailings. Using tailings from the Pulang Copper Mine in Yunnan Province, China, the mechanical properties and micro-mechanism of solidified samples with different contents of hydantoin epoxy resin and different curing time were measured. In addition, the effects of hydantoin epoxy resin on the characteristics and solidification mechanism were studied relative to the microstructure and mineral composition of the tailings solidified body.

2 Experimental

2.1 Materials and specimen preparation

2.1.1 Materials

The tailings were sampled from the tailings pond of the Pulang Copper Mine in Yunnan Province, China. Prior to the experiment, the copper tailings were dried at 105 °C in an electrothermal constant-temperature dry box for 12 h. The physical and mechanical properties of the tailings were tested in accordance with the ASTM E1856—97(2002) standard. The results are presented in Table 1. The hydantoin resin epoxy N,N- dicyclopropyl dimethylacetimide (C₉H₁₀N₂O₄R₁R₂, Wuxi Meihua Chemical Solvent Co., Ltd., Wuxi, China) and the solidifying activator 3,3'-diaminodipropylamine (DPTA) (C₆H₁₇N₃, Tokyo Chemical Industry Co., Ltd., Japan) form a gel system.

Table 1 Basic physical and mechanical properties of tailings

Property	Value
Specific gravity, G_s	2.69
Natural water content/%	15.22
Natural void ratio	0.63
Cohesion, c /kPa	1.76
Internal friction angle, ϕ /(°)	11.55
Angle of repose/(°)	33.08

2.1.2 Specimen preparation

The compositions of the S/S specimens are presented in Table 2. The quantity of additional hydantoin epoxy resin was between 0 and 30 wt.% in this study, and the DPTA/hydantoin epoxy resin mass ratio of 1/20 was chosen. The DPTA/hydantoin epoxy resin mass ratio was kept constant in all formulations. Distilled water was used throughout the experiment. The water/tailings mass ratio (0.29) was kept constant in all specimens. The S/S specimens were prepared using the following steps.

(1) Hydantoin epoxy resin and distilled water were fully mixed, and the copper mine tailings were added to the mixture.

(2) After a homogeneous mixture was achieved, it was fully mixed with distilled water, tailings, and hydantoin epoxy resin. The DPTA was added to the mixture after 5 min of mixing.

(3) The homogeneous mixture was molded into cylindrical molds with 100 mm in height and 50 mm in diameter. The specimens were cured in an electrothermal constant-temperature dry box at 60 °C for 1, 3, 5, 7 and 14 d, respectively before the characterization [37].

2.2 Test method

2.2.1 Grain size, XRD and XRF measurements

The grain size distributions of the tailings specimens were obtained using the wet laser method. An automatic laser particle size analyzer (MS2000), operated at 50 Hz and 200 W, was used along with a He–Ne gas laser source ($\lambda=633$ nm). The measuring range was 0.02–2000 μm , and the maximum detection angle was 135°.

The copper tailings and solidified body specimens were placed in stainless steel specimen holders for the X-ray diffractometer (XRD) analysis. A 9 kW rotating anode X-ray diffraction source, Smart Lab (Science and Technology Co., Ltd., Japan), operated at 30 mA and 40 kV, was employed. The XRD analysis was performed with Cu $K\alpha$ radiation ($\lambda=0.15416$ nm) with 2θ values from 10° to 90° at a scanning speed of 5 (°)/min. The JCPDS PDF database was used for the phase identification.

The tailings specimens were pressed into a thin sheet for the X-ray fluorescence (XRF) analysis. A 4 kW rotating anode X-ray fluorescence source, Axios mAX (Panalytical, Netherlands), operated at 160 mA and 60 kV, was employed. The element analysis was focused on Na–U, and the reproducibility of the angle measurement equipment was 0.0001°.

2.2.2 Mechanical properties test

The mechanical properties of the specimens were tested in accordance with the Chinese National Standard GB/T 50123—2019. The average compressive strengths of three replicates after specific curing periods were determined using a universal testing machine (XBD53056, Shanghai Xinbiao Testing Instrument Manufacturing Co., Ltd., China) operated at the speed of 1 mm/min.

Table 2 Chemical compositions of specimens

Specimen	Tailings (TS) content/wt.%	Hydantoin epoxy resin (HER) content ($m_{\text{HER}}/m_{\text{TS}}$)/%	DPTA content ($m_{\text{DPTA}}/m_{\text{HER}}$)/%	Water/TS mass ratio
TS/HER_0	100	0	5	0.29
TS/HER_2	100	2	5	0.29
TS/HER_5	100	5	5	0.29
TS/HER_10	100	10	5	0.29
TS/HER_20	100	20	5	0.29
TS/HER_30	100	30	5	0.29

2.2.3 Microstructure test

The microstructure of the specimens was studied by using scanning electron microscopy (SEM). The reaction of the crushed specimens was restricted using acetone, and then the specimens were impregnated into an epoxy resin under vacuum. The hardened specimens in the epoxy resin were polished and coated with carbon before SEM analysis. The morphological observations were performed using SEM (Tescan, Mira3 LMH, Czech Republic) at an accelerating voltage of 10 kV and working distance of approximately 8 mm.

3 Results

3.1 Characterization

The grain size distributions of the tailings and solidified specimens used in this work are illustrated in Fig. 1, which indicates that the specimens were mainly composed of silt and fine tailings. Furthermore, fine-grained soil (smaller than 75 μm) comprised 84.3% of the total specimen. The uniformity coefficient was greater than 5, and the curvature coefficient was less than 1. According to the particle size distribution, the tailings used in the test were fine tailings. After solidification, the grain size distribution curve of TS/HER_10 (Fig. 1) was similar to that of the tailings. The number of fine particles with size $<50 \mu\text{m}$ decreased slightly and the characteristic medium diameter (D_{50}) fell to 64% compared with those of the tailings. These results were an indication of homogenization for the tailings and solidified body.

The XRD patterns of the tailings and solidified specimen used in this work are illustrated in Fig. 2.

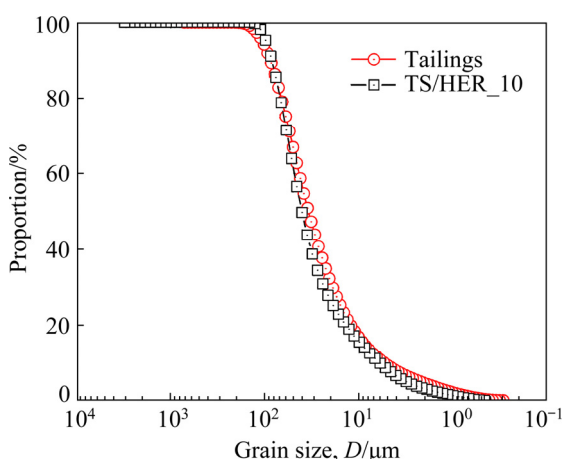


Fig. 1 Grain size distributions of tailings before and after solidification

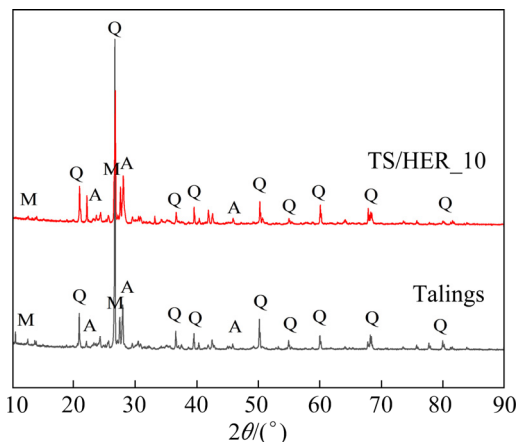


Fig. 2 XRD patterns of tailings and solidified TS/HER_10 (A: Anorthite; M: Microcline; Q: Quartz)

The major mineral phases of the tailings and TS/HER_10 were quartz, anorthite, and microcline. The above three minerals were found in all specimens. With higher content of hydantoin epoxy resin, the main phases of the initial mine tailings remained unchanged and there were no changes in the phase compositions of the specimens. After solidification, the mineral phase reflections decreased significantly, especially for the silicate minerals such as anorthite and microcline (Fig. 2).

The chemical compositions of tailings and the TS/HER_10 were determined using XRF, and the results are shown in Table 3. The main chemical components of tailings were SiO_2 , Al_2O_3 , K_2O , and CaO , which constituted up to 87.314% of the material. Similarly, the main chemical components

Table 3 Main chemical compositions of tailings and TS/HER_10

Chemical composition	Content/wt.-%	
	Tailings	TS/HER_10
SiO_2	64.876	56.536
Al_2O_3	13.946	10.972
K_2O	4.42	7.941
CaO	4.072	5.874
Na_2O	2.936	1.482
MgO	2.874	2.254
P_2O_5	1.122	0.937
CuO	0.086	0.024
MnO	0.030	0.023
Cr_2O_3	0.022	0.018
NiO	0.014	0.004

of TS/HER_10 amounted for 81.323%. With higher content of hydantoin epoxy resin, the main phases of the initial mine tailing powder continued to occur. However, the contents of SiO_2 and Al_2O_3 decreased, whereas the contents of K_2O and CaO increased in TS/HER_10, which supported the inference that the solidification process changes the main chemical compositions of tailings. Moreover, some heavy metals such as Cu, Mn, Cr, and Ni were found in TS/HER_10.

3.2 Effect of hydantoin epoxy resin content on strength of solidified body

The stress–strain curves of the solidified body with 0, 2, 5, 10, 20, and 30 wt.% hydantoin epoxy resin are shown in Fig. 3. The curing time of the solidified body was 7 d.

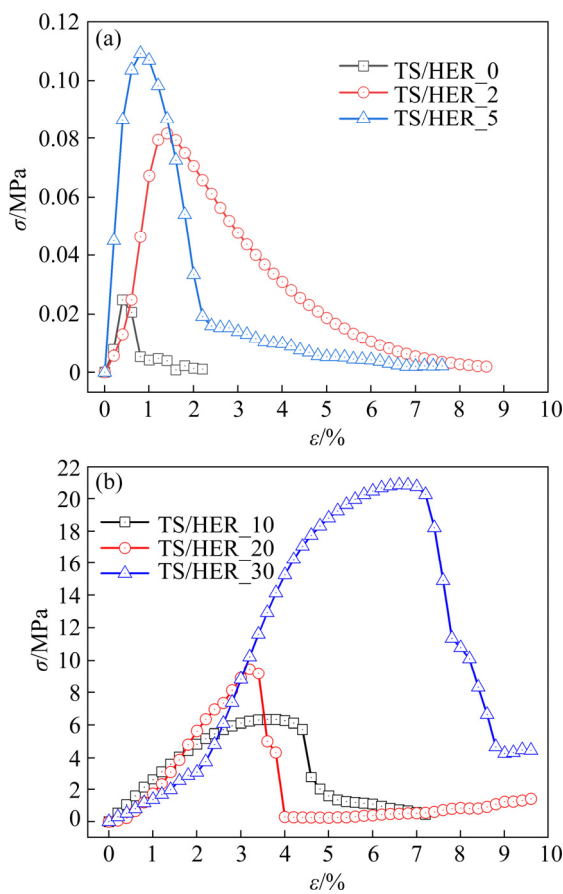


Fig. 3 Stress–strain curves of solidified body with different additions of hydantoin epoxy resin: (a) 0, 2, and 5 wt.% hydantoin epoxy resin; (b) 10, 20, and 30 wt.% hydantoin epoxy resin

As shown in Fig. 3(a), the curves were steep in the early stage, which indicated that the rate of stress growth was much greater than that of strain.

Compared with Fig. 3(a), Fig. 3(b) shows gentle curves in the early stage. Moreover, the stress–strain curves of specimens were very different, and when the solidified body reached the ultimate stress, the specimen failed, and the curves dropped sharply. By comparing the stress–strain curves of the solidified bodies with different compositions, it was found that with gradual increase in the hydantoin epoxy resin content, the declining portion of the stress–strain curves became steeper, indicating the increase in the brittleness of the solidified body and the decrease in its plasticity.

At the same time, it was concluded from Fig. 3 that the stress–strain curves could be divided into 3 stages. The first stage was compaction, where the stress–strain curves were concave; the pores were closed by the action of pressure, and the deformation of the solidified body was larger. The second stage was elastic deformation, where the stress–strain curves were approximately a straight line. The stress increased linearly with the increase of the strain and reached its peak, because the porosity of the solidified body decreased and a dense structure was gradually acquired. The third stage was specimen failure, where the stress–strain curves dropped sharply, and the solidified body conspicuously displayed the phenomenon of stress reduction. The main reason was that the stress exceeded the yield stress of the solidified body, resulting in the destruction.

The relationship between failure strain and compressive strength of the solidified body with different hydantoin epoxy resin contents are shown in Fig. 4.

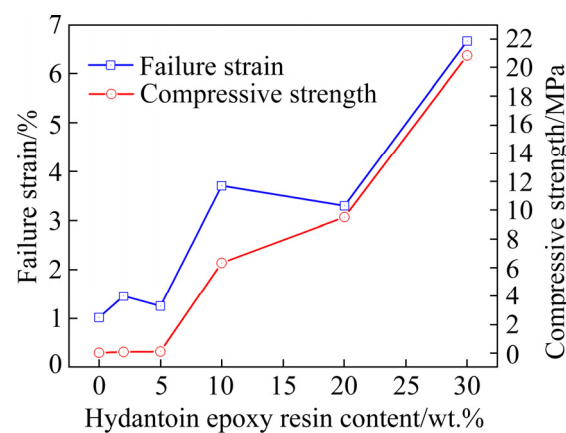


Fig. 4 Failure strain and compressive strength of solidified body with different hydantoin epoxy resin contents

As shown in Fig. 4, with the increase in the hydantoin epoxy resin content, the compressive strength and overall trend of failure strain increased. When the content of hydantoin epoxy resin increased from 0 to 5 wt.%, the compressive strength increased from 0.03 to 0.11 MPa, and the failure strain increased from 1.02% to 1.25%. The results showed that the compressive strength of the solidified body increased by about 2.7 times, but the range of increase was small. The compressive strengths of the 0, 2, and 5 wt.% solidified specimens were small, because the effect of the hydantoin epoxy resin gel system on the stress-strain characteristics of the tailings was not obvious. When the hydantoin epoxy resin content increased from 5 to 30 wt.%, the compressive strength increased from 0.11 to 20.84 MPa, and the failure strain increased from 1.25% to 6.66%. The results showed that the compressive strengths of the solidified increased by about 188.5 times. The compressive strengths of the 10, 20, and 30 wt.% solidified specimens increased significantly, because with increase in the content of hydantoin epoxy resin, the hydantoin epoxy resin gel system became increasingly reactive with tailings. The granulation of the gel system and tailings was strengthened. The gel system and tailings formed a stronger skeletal structure and provided a better overall structure of the solidified body. Similar phenomenon was observed by WANG et al [38]. Thus, higher hydantoin epoxy resin content resulted in a stronger solidified body, which alleviated the effect of the reaction of the hydantoin epoxy resin gel system on the compressive strength. Therefore, low content of the hydantoin epoxy resin should be avoided in the actual solidification treatment of tailings, as it is detrimental to the strength of the solidified body. Considering the strength and economy of the solidified body, the appropriate hydantoin epoxy resin content is about 10 wt.%.

3.3 Effect of curing time on strength of solidified body

The stress-strain curves of the solidified specimens at different curing time are shown in Fig. 5. The specimen with 10 wt.% hydantoin epoxy resin was selected.

As shown in Fig. 5, the stress-strain curves of the solidified specimens at different curing time

were very different. The curve of the specimen with curing time of 1 d was relatively flat. This indicated that the curing time of 1 d was relatively short; therefore, the hydantoin epoxy resin gel system was unable to fully respond, and the strength growth was delayed. The curves for the specimens with curing time of 3, 5, 7, and 14 d were steep. When the curing time was more than 1 d, the gel system increased gradually with increase in the curing time. The peak value of the stress-strain curve increased, and the changes in the rising and falling stages of the curves were more significant. The strength of the solidified body increased faster at the curing time of 7 and 14 d. In addition, based on the comparison of the curves in Fig. 5, it was found that the stress-strain curves of 3 and 5 d, and 7 and 14 d, showed similar trends, respectively. Among them, the difference in compressive strength between the solidified body cured for 3 and 5 d was small, because the reaction speed of the gel system slowed down and the strength increased slowly during the curing time of 5 d. However, the difference for 7 and 14 d was smaller because at 7 d, the gel system reaction entered the end stage; the strength of the solidified body increased slightly when the curing time was increased to 14 d. It was concluded that the curing time was also a controlling factor for compressive strength.

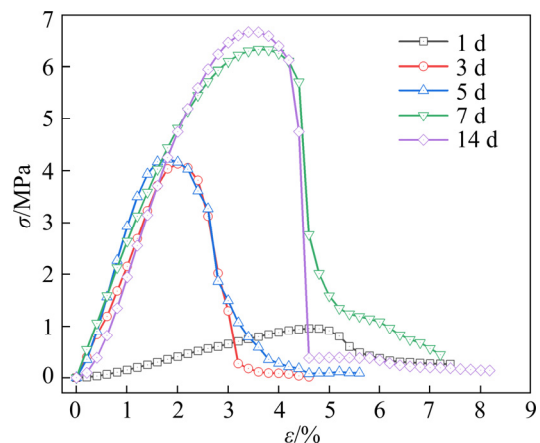


Fig. 5 Stress-strain curves of solidified body (TS/HER_10) at different curing time

The variations in the failure strain and compressive strength of the solidified body (TS/HER_10) at different curing time are shown in Fig. 6.

As shown in Fig. 6, with the increase in the curing time, the compressive strength increased,

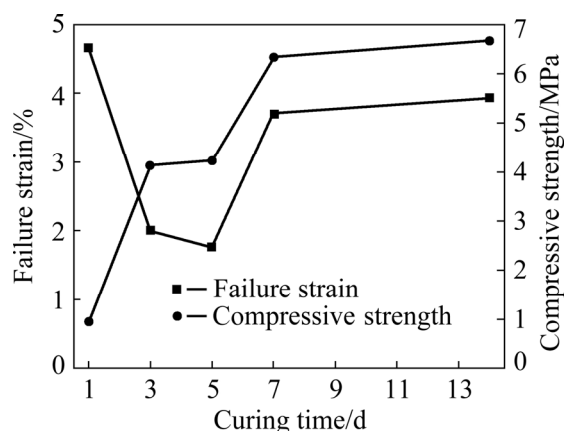


Fig. 6 Failure strain and compressive strength of solidified body (TS/HER_10) at different curing time

and the failure strain decreased at first and then increased, which indicated that the hydantoin epoxy gel system had excellent early strength and fast hardening. The compressive strength of the specimen with shorter curing time (1–5 d) increased from 0.95 to 4.22 MPa, which was increased by 3.44 times, and the failure strain decreased from 4.66% to 1.76%. The compressive strength of the specimen with longer curing time (5–7 d) was increased by 0.5 times from 4.22 to 6.33 MPa, and the failure strain increased from 1.76% to 3.71%. The reason was that gel reaction between the hydantoin epoxy resin and solidifying activator occurred on the tailings. The agglomeration and hardening reaction between them are complex and time consuming. Similar findings were observed by LI et al [39,40]. When the curing time was less than 5 d, the reaction between the epoxy resin and solidifying activator occurred continuously. Therefore, the compressive strength was larger and failure strain was smaller at the curing time of 5 d. With increase in curing time, the aggregates generated during the early reaction connected the soil particles to form a planar mosaic structure, which reduced the pores in the solidified body and further increased the cohesive force between the soil particles. Owing to the increase in curing time, the gel reaction gradually extended to the latter part. Therefore, when the curing time increased from 7 to 14 d, the compressive strength increased slowly, and the failure strain exhibited the same tendency.

3.4 Microstructure of solidified specimens

Microstructures of the solidified specimens

added with 0, 2, 5, 10, 20, and 30 wt.% hydantoin epoxy resin are shown in Fig. 7.

From Fig. 7(a), when the hydantoin epoxy resin content was 0, there was no cementation in the solidified body, and the entire body was composed of regular layers with obvious stratification. Because of the absence of hydantoin epoxy resin, the gelation reaction did not occur. The degree of cementation between the soil particles was weak, which resulted in low compressive strength. From Fig. 7(b), when the hydantoin epoxy resin content was 2 wt.%, a small amount of cementation was formed on the surface of the solidified body, which encapsulated the soil particles and gradually made the layered structure compact. Moreover, the difference in the surface particle size was obvious, i.e., irregular block and granular particle, with a number of pores, and the overall structure of the solidified body was loose. From Fig. 7(c), when the hydantoin epoxy resin content was 5 wt.%, cementation increased continuously, and the soil particles were tightly wrapped. Irregularly shaped aggregates were distributed on the surface. Pores of large sizes were obviously reduced, and some small pores existed. Massive cement particles were scattered on the surface of the solidified body, and some particles were stacked in clusters to form large blocks. From Fig. 7(d), when the hydantoin epoxy resin content was 10 wt.%, the cementation in the solidified body was overlapped and arranged closely. The pores of the soil particles were sealed, and the overall surface was smooth. The cement particles closely adhered to each other to form a connected whole, which limited the deformation of the soil particles in the solidified body. Thus, the integrity and stability of the entire solidified body were improved, resulting in a significant increase in the strength. From Fig. 7(e), when the hydantoin epoxy resin content was 20 wt.%, the resin gel system generated excessive gel material on the surface of the solidified body. This excessive gel material was a lump-shaped aggregate, irregularly distributed and stacked on the surface of the solidified body. From Fig. 7(f), when the hydantoin epoxy resin content was 30 wt.%, the superfluous gel material generated by the hydantoin epoxy resin gel system formed a cluster, which was closely arranged on the surface of the solidified body. The presence of the gel material in the solidified body further enhanced the strength of the solidified body.

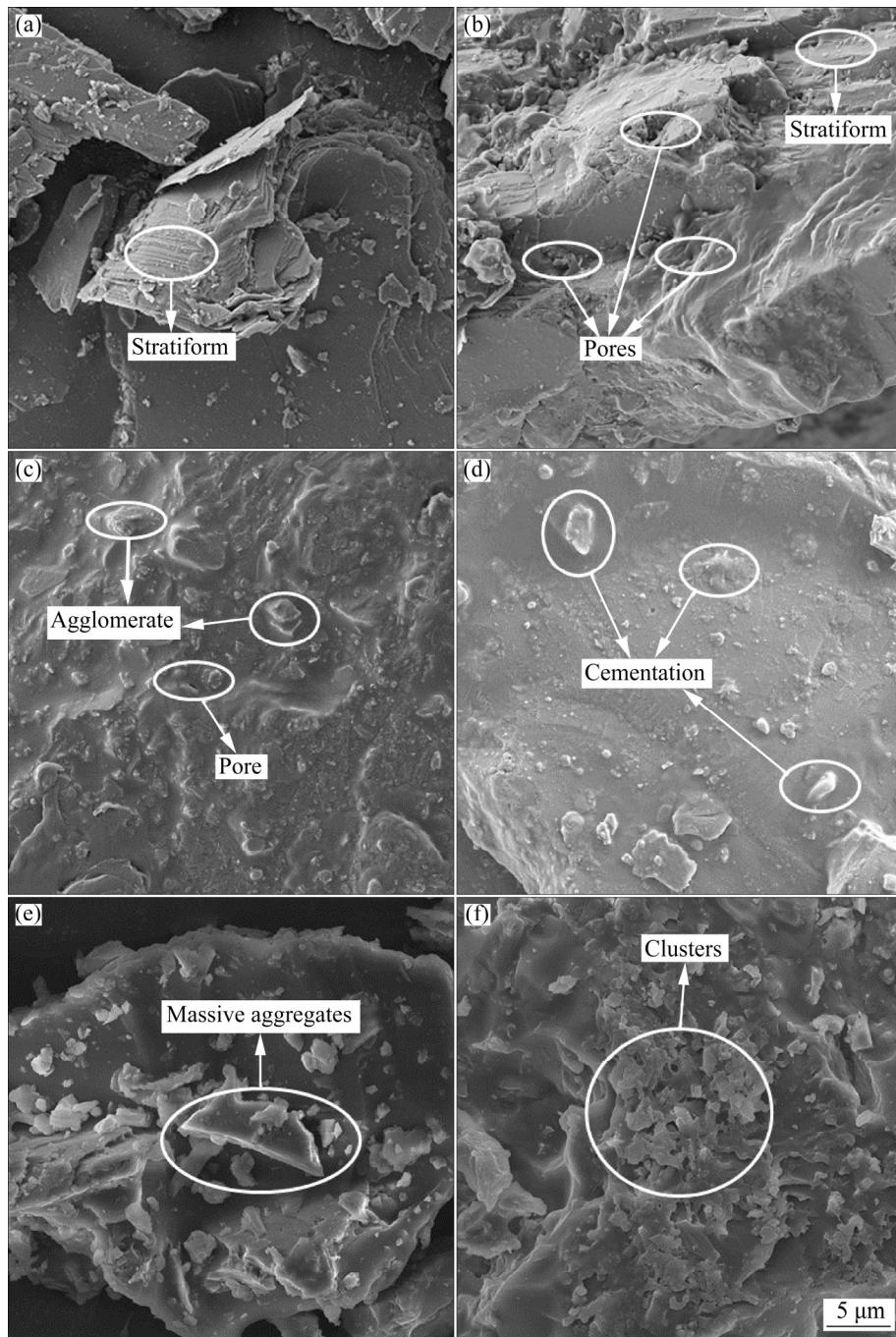


Fig. 7 Microstructures of solidified specimens: (a) TS/HER_0; (b) TS/HER_2; (c) TS/HER_5; (d) TS/HER_10; (e) TS/HER_20; (f) TS/HER_30

From Figs. 7(e) and (f), it was concluded that the morphology and distribution of the gel material had considerable influence on the compressive strength of the solidified body.

4 Discussion

The grain size distributions of the tailings and TS/HER_10 revealed the gelation reaction between

hydantoin epoxy resin and tailings (Fig. 1). The gelation reaction made the particle size increase slightly. The patterns revealed that the increase of the particle size of the solidified body provided a precondition for the improvement of the mechanical properties. The XRF result revealed that the gel reaction would change the chemical compositions of the tailings and form the clusters. And the clusters ensured the mechanical properties of the

solidified body.

The XRD patterns revealed that the raw tailings and solidified body had high crystallinity (Fig. 2). The major mineral phases of the tailings were quartz, anorthite, and microcline (Fig. 2). After solidification treatment, the major mineral phases of the solidified body (anorthite and microcline) were changed. The decrease in the mineral phase reflection intensity was a manifestation of the amorphization. It was concluded that the reaction of the hydantoin epoxy resin gel system could change the mineral phases of tailings. However, the gel system cannot create new substances. The compressive strength of the solidified body originated from the gelling reaction between the hydantoin epoxy resin gel system and tailings.

From the microstructure of the solidified body, it was concluded that with the increase in the hydantoin epoxy resin content from 0 to 30 wt.%, the tailings particles and gel systems became closely interrelated. Most of the debris particles were surrounded by the gel system, formed stable aggregates, and filled the pores. Thus, strong structural bonds were created. In addition, the “granular-mosaic-cementation” structure was produced, which had higher strength and significantly improved the strength of the solidified body. In addition, when the hydantoin epoxy resin content was 10 wt.%, the cementation increased gradually, and the granulation was strengthened. The cementation significantly improved the bonding force between the soil particles and promoted the deformation resistance ability of the solidified body. Moreover, the compressive strength of TS/HER_10 reached 6.33 MPa, thus meeting the requirement for its application as subgrade bed filling [5]. Further, the compressive strengths of TS/HER_20 and TS/HER_30 were 9.52 and 20.84 MPa, respectively. This phenomenon was attributed to the formation and accumulation of clusters (Figs. 7(e) and (f)), which greatly improved the strength of the solidified body. However, in the treatment process of actual tailings, it is not recommended to use the hydantoin epoxy resin contents of 20 and 30 wt.%, considering the economic benefits.

It can be concluded from Figs. 5, 6, and 7(d) that the reaction of the hydantoin epoxy resin gel

system requires certain curing time to ensure the completeness of the reaction and formation of a connected mass. Moreover, the strength of the solidified body specimens cured for 14 d was only 0.34 MPa higher than that of specimens cured for 7 d. In the case of TS/HER_10 specimen with 7 d of curing time, the compressive strength was 6.33 MPa, which could satisfy the Specifications for Design of Highway Subgrades defined by JTGD30-2015. Although the strength of the specimens with 14 d of curing time was slightly improved, the process requires more time and energy. Therefore, from the perspectives of economics and mechanical strength, the optimal curing time was chosen to be 7 d.

The reaction between the hydantoin epoxy resin and the solidifying activator has resulted in a reduction in the pores between the particles of the tailings. The pore structure distribution has been optimized, forming a solidified body to facilitate the formation of the macro strength. The strength of the cement-solidified tailings is mostly dependent on the C—S—H gel generated by hydration of the cement.

For the same tailings, the solidifying cost of hydantoin epoxy gel system is 1.78 times that of cement and specific results are shown in Table 4. Moreover, WAN et al [5] found that the strength of tailings solidified body with 50% P.C 32.5 cement was only 0.6 MPa, which could not be put into engineering practice. To achieve the same mechanical strength as the hydantoin epoxy gel system, a substantial increase in cement addition is required. However, increasing the amount of cement will not only lead to the compatibility of solidified body, violate the principle of reducing the utilization of tailings, but also increase the economic cost. Based on the engineering application and economic benefits, the optimal mixing ratio of the hydantoin epoxy gel system can be explored in engineering practice.

Table 4 Cost comparison of different solidified materials

Solidifying material	Mixing content/%	$\sigma/$ MPa	Cost/ (RMB \cdot t $^{-1}$)
Hydantoin epoxy resin gel system	10	6.33	800
P.C 32.5	50 [5]	0.6	450

5 Conclusions

(1) The characterization revealed nearly no difference between tailings and TS/HER_10. The grain size distributions, mineral phases, and chemical compositions were similar.

(2) The hydantoin epoxy resin significantly improved the mechanical properties of the solidified body. When the hydantoin epoxy resin content increased from 5 to 30 wt.%, the compressive strength of the solidified body was increased by 188.5 times, and the failure strain increased from 1.25% to 6.66%.

(3) The reaction of the hydantoin epoxy resin gel system requires certain curing time to ensure full reaction. With the increase in curing time, the peak value of the stress-strain curve increased significantly. When the curing time increased from 1 to 5 d, the compressive strength was increased by 3.44 times, and the failure strain decreased from 4.66% to 1.76%.

(4) The tailings particles and gel systems were closely interrelated. With the increase in content of hydantoin epoxy resin, the “granular-mosaic-cementation” structure was produced, which greatly enhanced the strength of the solidified body.

Acknowledgments

The authors are grateful for financial support from the National Natural Science Foundation of China (Nos. 41972282, 41807253), the Natural Science Foundation of Hunan Province, China (No. 2021JJ30804), and the Research Fund Program from Yunnan Diqing Nonferrous Metal Co., Ltd., China (No. DQYS-ZYB-09-(2021)001).

References

[1] CAI Yong-bing, SHAO Li, FAN Xing-jun, LI Fei-yue, MENG Fan-de, ZHANG Hua. Study on the release and vertical migration characteristics of As and Sb in farmland soil contaminated by dam break of Huashan tailings pond, Anhui, China [J]. Environmental Chemistry, 2020, 39(9): 2479–2489. (in Chinese)

[2] HE Y, LI B B, ZHANG K N, LI Z, CHEN Y G, YE W M. Experimental and numerical study on heavy metal contaminant migration and retention behavior of engineered barrier in tailings pond [J]. Environmental Pollution, 2019, 252: 1010–1018.

[3] SUN Z H, XIE X D, WANG P, HU Y A, CHENG H F. Heavy metal pollution caused by small-scale metal ore mining activities: A case study from a polymetallic mine in South China [J]. Science of the Total Environment, 2018, 639: 217–227.

[4] HE Y, LI Z, ZHANG K N, YE W M, CHEN Y G. Effect of CuSO₄ on the hydromechanical behavior of compacted tailings [J]. Mine Water and the Environment, 2020, 39: 103–111.

[5] WAN Lei, ZHANG Zhi, SONG Hua-song, WANG Xu-dong, WANG Dong-lin. Effect of drying and wetting cycles on strength characteristic of alkali-activated materials solidified fine iron tailings sand [J]. Bulletin of the Chinese Ceramic Society, 2020, 39(7): 2223–2231. (in Chinese)

[6] LI P, CAI M F. Challenges and new insights for exploitation of deep underground metal mineral resources [J]. Transactions of Nonferrous Metals Society of China, 2021, 31(11): 3478–3505.

[7] CHEN Q Y, TYRER M, HILLS C D, YANG X M, CAREY P. Immobilisation of heavy metal in cement-based solidification/stabilisation: A review [J]. Waste Management, 2009, 29(1): 390–403.

[8] SALIHOGLU G. Immobilization of antimony waste slag by applying geopolymerization and stabilization/solidification technologies [J]. Journal of the Air & Waste Management Association, 2014, 64(11): 1288–1298.

[9] WAN Q, RAO F, SONG S X, ZHANG Y M. Immobilization forms of ZnO in the solidification/stabilization (S/S) of a zinc mine tailing through geopolymerization [J]. Journal of Materials Research and Technology, 2019, 8(6): 5728–5735.

[10] HILLS C D, POLLARD S J T. The influence of interferences effect on the mechanical, microstructural and fixation characteristics of cement solidified hazardous waste forms [J]. Journal of Hazardous Materials, 1997, 52(2/3): 171–191.

[11] HE Y, WANG M M, WU D Y, ZHANG K N, CHEN Y G, YE W M. Effects of chemical solutions on the hydromechanical behavior of a laterite bentonite mixture used as an engineered barrier [J]. Bulletin of Engineering Geology and the Environment, 2021, 80(2): 1–12.

[12] KIVENTERÄ J, PIEKKARI K, ISTERI V, OHENOJA K, TANSKANEN P, ILLIKAINEN M. Solidification/stabilization of gold mine tailings using calcium sulfoaluminate–belite cement [J]. Journal of Cleaner Production, 2019, 239: 118008.

[13] HUANG X, HUANG T, LI S, MUHAMMAD F, XU G J, ZHAO Z Q, YU L, YAN Y J, LI D W, JIAO B Q. Immobilization of chromite ore processing residue with alkali-activated blast furnace slag-based geopolymer [J]. Ceramics International, 2016, 42(8): 9538–9549.

[14] CHEN I A, HARGIS C W, JUENGER M C G. Understanding expansion in calcium sulfoaluminate–belite cements [J]. Cement and Concrete Research, 2012, 42(1): 51–60.

[15] HUANG X, ZHUANG R L, MUHAMMAD F, YU L, SHIAU Y, LI D W. Solidification/stabilization of chromite ore processing residue using alkali-activated composite cementitious materials [J]. Chemosphere, 2017, 168: 300–308.

[16] JIMÉNEZ A, PRIETO M. Thermal stability of ettringite exposed to atmosphere: Implications for the uptake of harmful ions by cement [J]. Environmental Science &

Technology, 2015, 49: 7957–7964.

[17] LEE N K, LEE H K. Reactivity and reaction products of alkali-activated, fly ash/slag paste [J]. Construction and Building Materials, 2015, 81: 303–312.

[18] XIA M, MUHAMMAD F, ZENG L H, LI S, HUANG X, JIAO B Q, SHIAU Y, LI D W. Solidification/stabilization of lead-zinc smelting slag in composite based geopolymers [J]. Journal of Cleaner Production, 2019, 209: 1206–1215.

[19] ZHAO S J, XIA M, YU L, HUANG X, JIAO B Q, LI D W. Optimization for the preparation of composite geopolymers using response surface methodology and its application in lead-zinc tailings solidification [J]. Construction and Building Materials, 2021, 266: 120969.

[20] AHMARI S, ZHANG L Y. Production of eco-friendly bricks from copper mine tailings through geopolymers [J]. Construction and Building Materials, 2012, 29: 323–331.

[21] JIAO X K, ZHANG Y M, CHEN T J, BAO S X, LIU T, HUANG J. Geopolymerisation of a silica-rich tailing [J]. Minerals Engineering, 2011, 24(15): 1710–1712.

[22] MAHADEVA RAJU G K, MADHU G M, KHAN M A, REDDY P D S. Characterizing and modeling of mechanical properties of epoxy polymer composites reinforced with fly ash [J]. Materials Today: Proceedings, 2018, 5(14): 27998–28007.

[23] KUMAR N N, SIDDESHCHINCHOL I, HEGDE P R, SHIVAGIRI S Y, REVANASIDDAPPA M. Synthesis and characterization of fly ash/wooden fiber reinforced epoxy resin polymer composite [J]. Materials Today: Proceedings, 2018, 5(1): 501–507.

[24] JIANG C, GAN X P, ZHANG D, XIE R, ZHOU K C. Gelcasting of aluminum nitride ceramics using hydantoin epoxy resin as gelling agent [J]. Ceramics International, 2013, 39(8): 9429–9433.

[25] JUNG Y S, PAIK U, PAGNOUX C, JUNG Y G. Consolidation of aqueous concentrated silicon nitride suspension by direct coagulation casting [J]. Materials Science and Engineering A, 2003, 342(1/2): 93–100.

[26] MAO X J, SHIMAI S, DONG M J, WANG S W. Investigation of new epoxy resins for the gel casting of ceramics [J]. Journal of the American Ceramic Society, 2008, 91(4): 1354–1356.

[27] ZENG W M, GAN X P, LI Z Y, ZHOU K C. The preparation of silicon nitride ceramics by gelcasting and pressureless sintering [J]. Ceramics International, 2016, 42(10): 11593–11597.

[28] XIE R, ZHANG D, ZHANG X Y, ZHOU K C, BUTTON T W. Gelcasting of alumina ceramics with improved green strength [J]. Ceramics International, 2012, 38(8): 6923–6926.

[29] CHINDAPRASIRT P, CHAREERAT T, SIRIVIVATNANON V. Workability and strength of coarse high calcium fly ash geopolymers [J]. Cement and Concrete Composites, 2007, 29(3): 224–229.

[30] MUHAMMAD F, HUANG X, LI S, XIA M, ZHANG M L, LIU Q, SHEHZAD HASSAN M A, JIAO B Q, YU L, LI D W. Strength evaluation by using polycarboxylate superplasticizer and solidification efficiency of Cr^{6+} , Pb^{2+} and Cd^{2+} in composite based geopolymers [J]. Journal of Cleaner Production, 2018, 188: 807–815.

[31] LI N, LV S W, WANG W, GUO J, JIANG P, LIU Y. Experimental investigations on the mechanical behavior of iron tailings powder with compound admixture of cement and nano-clay [J]. Construction and Building Materials, 2020, 254: 119259.

[32] LIU J J, ZHA F S, XU L, KANG B, YANG C B, FENG Q, ZHANG W, ZHANG J W. Strength and microstructure characteristics of cement-soda residue solidified/stabilized zinc contaminated soil subjected to freezing-thawing cycles [J]. Cold Regions Science and Technology, 2020, 172: 102992.

[33] YU Z, SHI X Z, CHEN X, ZHOU J, QI C C, CHEN Q S, RAO D J. Artificial intelligence model for studying unconfined compressive performance of fiber-reinforced cemented paste backfill [J]. Transactions of Nonferrous Metals Society of China, 2021, 31(4): 1087–1102.

[34] ZHAO S X, WANG G R, YANG H Y, CHEN G B, QIU X M. Agglomeration-aggregation and leaching properties of mechanically activated chalcopyrite [J]. Transactions of Nonferrous Metals Society of China, 2021, 31(5): 1465–1474.

[35] MUHAMMAD F, XIA M, LI S, YU X, MAO Y H, MUHAMMAD F, HUANG X, JIAO B Q, YU L, LI D W. The reduction of chromite ore processing residues by green tea synthesized nano zerovalent iron and its solidification/stabilization in composite geopolymers [J]. Journal of Cleaner Production, 2019, 234: 381–391.

[36] ZHAO Ze-min, CHEN Wei, LI Qiu, YUAN Sen-sen, PENG Rao. Effect of fine tailings on the strength properties and microstructure of tailings backfill [J]. Journal of Wuhan University of Technology, 2018, 40(6): 16–21. (in Chinese)

[37] ZHAO Yang, XIE Rui, ZHANG Yan, ZHOU Ke-chao, ZHANG Dou. Gelcasting of lead zirconate titanate prepared by water-soluble epoxy resin [J]. The Chinese Journal of Nonferrous Metals, 2014, 24(3): 773–778. (in Chinese)

[38] WANG Bing, YANG Wei-min., LI Zhan-qiang. Micromechanism of strength increase with curing time for compacted cement-soil [J]. Journal of University of Science and Technology Beijing, 2008, 30(3): 233–238. (in Chinese)

[39] LI Ling, XIN Ya-quan, QIN Xu-feng, TIAN Jin-li, CHEN Jian-nan. Curing kinetic of hydantoin epoxy/HHPA system by non-isothermal data [J]. Surface Technology, 2018, 47(1): 230–235. (in Chinese)

[40] LI X Y, WANG Z Q, WANG J W, JING X, HUANG J J, LI L, MEI Y G, LI W Z, FANG Y T. Acid-leaching and silanization of catalytic gasification ash enhance the mechanical properties of polyurethane/ash composites [J]. Industrial & Engineering Chemistry Research, 2019, 58(3): 1426–1433.

海因环氧树脂固化铜尾矿的力学性能及微观结构演变

贺 勇^{1,2}, 蒋文强^{1,2}, 陈科平^{1,2}, 吴练荣³, 张可能^{1,2}, 喻志鹏^{1,2}, 甘雪萍⁴, 冯德山^{1,2}

1. 中南大学 有色金属成矿预测与地质环境监测教育部重点实验室, 长沙 410083;
2. 中南大学 地球科学与信息物理学院, 长沙 410083;
3. 云南迪庆有色金属有限责任公司, 香格里拉 674400;
4. 中南大学 粉末冶金国家重点实验室, 长沙 410083

摘要: 基于强度和微观试验, 系统研究海因环氧树脂掺量和养护龄期对铜尾矿试样力学性能及微观结构的影响规律。结果表明, 当海因环氧树脂掺量为 30% (质量分数)时, 固化体试样强度达到 20.84 MPa。当海因环氧树脂掺量为 10% (质量分数)的固化体的养护龄期为 7 和 14 d 时, 其强度分别为 6.33 和 6.67 MPa, 均满足其作为基础填料和建筑材料的要求。微观试验结果表明, 随着海因环氧树脂掺量的增加, 团粒化作用加强, 固化体孔隙减少, 从而大大提高了固化体强度。

关键词: 铜尾矿; 海因环氧树脂; 力学性能; 微观结构

(Edited by Wei-ping CHEN)